Robotic Fastening with a Manual Screwdriver

Ling Tang Yan-Bin Jia
Department of Computer Science
Iowa State University
Ames, IA 50010, USA
ling,jia@iastate.edu

Abstract— **The robotic hand is still no match for the human hand on many skills. Manipulation of hand tools, which usually requires sophisticated finger movements and fine controls, not only poses a clear technical challenge but also carries a great potential for enabling the same robot to assist humans in a wide range of tasks accomplishable using tools. This paper takes a first step to investigate how a robotic arm mounts a rigidly attached screwdriver onto a screw (positioned in a tapped hole) and then tightens it using the tool. Mounting begins with sliding the screwdriver's tip on the screw's head along preplanned paths to search for the drive and follows with rotations of the screwdriver to drop the tip into the drive. Prevention of a slip off the screw's head is achieved via using impedance to install a "virtual fence" along its edge. Turning of the screw is conducted via hybrid position/admittance control based on modeled reaction forces between the screw and the substrate. Simulation results with a Kuka Arm demonstrate the smoothness of the entire action.**

I. Introduction

Decades of research has made significant progress on robotic grasping [1] and dexterous manipulation [2], [3]. The skill level of robotic hands today is nevertheless limited in that many fine manipulation tasks are still beyond their reach. Although such a hand is most likely targeted for work or assistance in the human environment, tasks configured for everyday life are often solved using hand tools. Tool usage not only tests the hand's dexterity and versatility but also serves as a milestone for achievement of human-level dexterity. It has great potentials in home automation, where the robot can take over many chores, elderly assistance, where health care can become more cost-efficient as a result, and medical robotics, where robotic hands capable of maneuvering medical tools can reduce fatigue of doctors and nurses.

Robotic tool usage has been investigated for its different phases from tool recognition [4], [5] to tool grasping and orientation [6], [7], [8], [9], [10]. Although demonstrated on tasks such as bolt unscrewing [11], drilling [12], plant watering [13], etc., the level of exhibited dexterity has been primitive due to ignorance of friction, compliance, and control. Furthermore, hand tools have been mostly excluded because they demand maneuver skills.

Our attention on tool usage turns to fastening [14], which encompasses a broad class of tasks where fasteners such as screws, bolts, and nuts are used to hold objects together under the actions of torquing applied by tools such as screwdrivers and wrenches. Fastening is fundamental to industrial assembly and common in household tasks. Power tools such as electric screwdrivers and impact wrenches are fast and suited especially for high volume industrial productions. They are, however, also bulky (unable to reach a fastener within a very small space), limited (not to be used in the vicinity of conductive matter such as water), and in need of a setup.

In this paper, we investigate the task of screw driving by a robotic arm using a hand screwdriver with a focus on two maneuvers: insertion of the screwdriver tip into the drive of a screw and torquing of the screw to tightness. This preliminary investigation assumes that the screwdriver is rigidly mounted on the arm and the screw is pre-mounted but not tightened into a substrate. Pickups of the screwdriver and screw and pre-mounting of the latter by a robotic hand require complicated finger actions and dealing of issues such as cross threading and jamming, all of which are beyond the paper's scope. Alignment of two threaded parts before fastening has nevertheless been investigated based on vision [15], [16] or force and position feedback [17].

Insertion of the screwdriver tip can be viewed as a generalized version of the well-studied peg-in-hole problem [18], [19], [20], [21], [22]. Existing results, primiarly concerning cylindrical pegs and holes, are not easily adaptable to other shapes. In Section II, we present a strategy that first searches for the drive by moving the tip on the screw's head under hybrid control [23] in at most two passes. A virtual wall is installed around the head's boundary under impedance control [24] to prevent the tip from sliding off the boundary. As soon as the drive is encountered by the sliding tip, the screwdriver is first rotated compliantly against one of its edges until the tip is tangent to the edge, which then initiates a downward movement that will end with the tip in contact with the drive's bottom. A second rotation then aligns the tip's edge with the bottom to get the screwdriver ready for torquing.

The action of fastening has been investigated on modeling or analysis of the fastener-substrate interactions [25], [26], [27], [28], [29] and control of the fastener's motion [30], [31], [32], [33]. Section III studies control of the arm to perform screw driving through contacts at the screwdriver's tip and between the threads of the screw and the hole in the substrate. Contact force at the tip is measured by a

*Support for this research was provided in part by Iowa State University (ISU). The authors would like to thank Shengwen Xie for his initial effort and thoughts on the problem.

force/torque sensor connecting the arm's end-effector and the screwdriver. Contact force between threads can be estimated based on the analysis from [26] and from the current pose of the screwdriver. We describe a hybrid strategy that conducts position control along the axial direction to drive the screw forward and admittance control in the five other directions to keep the screwdriver and screw from deviating too much from the hole's axis.

Section V concludes the paper with a short summary and a discussion over future direction.

II. MOUNTING SCREWDRIVER ONTO SCREW

We assume that a screw has been pre-mounted into a threaded hole and is waiting to be tightened by a screwdriver. The first step is to mount the screwdriver's tip inside the screw's drive. For a typical slotted machine screw, the head diameter varies from 1 mm to 25 mm, and the drive width varies from 0.6 mm to 2.7 mm. It is almost impossible to accurately determine the exact position/orientation of the screw beforehand, and the robotic arm's control inaccuracy also increases the difficulty in operating the screwdriver within such a small range. Compliance between the screwdriver and the screw can be utilized to carry out the operation with force sensing available.

Suppose we have a robotic arm with n degrees of freedom (DOFs), whose end-effector has a rigidly mounted 6-DOF force/torque sensor. To operate a screwdriver, $n \geq 6$ must hold. We make the following assumptions:

- The screw remains stable inside the hole.
- Its pose is approximately known.
- The screw drive's orientation is unknown.

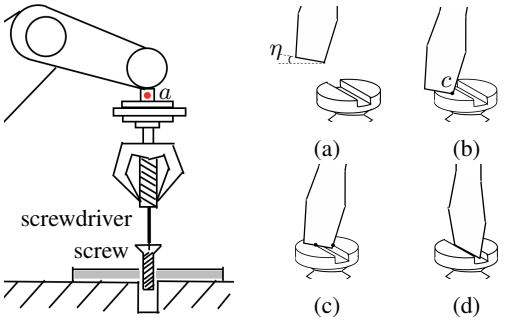

Fig. 1: Task setup and four snapshots of tip insertion into the drive: (a) initial configuration, where η is a small tilting angle of the screwdriver; (b) contact establishment and drive search; (c) tip in the drive; and (d) target configuration.

The action of mounting the screwdriver onto the screw is divided into three steps as shown in Fig. 1: establishing the contact between the screw and the screwdriver (a)–(b), searching for the screw drive (b)–(c), and rotating the screwdriver to insert the tip (c)–(d).

A. Contact Establishment

First, we move the screwdriver's tip down to touch the screw head's center, which is known with some error. During the movement, the screwdriver is tilted about its body y-axis (perpendicular to the shaft plane) for a small angle η (see Fig. 1(a)). This leads to a point-face contact with the screw head (see Fig. 1(b)). The action can be easily carried out under a proportional-integral-differential (PID) control over the screwdriver in the world frame $\{w\}$.

Denote $\boldsymbol{\theta}$ as the vector of n joint angles, $\boldsymbol{\tau}$ as the joint torque vector, and ρ_a as the 6-dimensional wrench vector (force and torque) exerted at a reference a on the arm's end-effector (see Fig. 1). The wrench ρ_a is read by the sensor after compensating the gravitational effects of the sensor and the screwdriver. The arm's dynamics is described in the joint space as follows:

$$\boldsymbol{\tau} = M(\boldsymbol{\theta})\ddot{\boldsymbol{\theta}} + C(\boldsymbol{\theta}, \dot{\boldsymbol{\theta}})\dot{\boldsymbol{\theta}} + N(\boldsymbol{\theta}) - J_a^\top \boldsymbol{\rho}_a \tag{1}$$

where $M(\boldsymbol{\theta})$ is the $n \times n$ mass matrix including the screwdriver and F/T sensor, $C(\boldsymbol{\theta}, \dot{\boldsymbol{\theta}})$ is the Coriolis and centrifugal term, $N(\boldsymbol{\theta})$ is the gravity term, and J_a is the $6 \times n$ Jacobian matrix at the end-effector.

We can define the state in the task space as $\boldsymbol{x} = (x, y, z, \alpha, \beta, \gamma)^\top$, where (x, y, z) represents the position of the screw-driver's tip (point c in Fig. 1) and (α, β, γ) are the z-y-x Euler angles to describe the screwdriver's orientation. We have $\dot{\boldsymbol{x}} = J_c\dot{\boldsymbol{\theta}}$, where J_c is the Jacobian that maps joint velocities to linear velocity and Euler angle rates at the contact point c in Fig. 1(b). Differentiating this velocity equation, we get

$$\ddot{\boldsymbol{\theta}} = J_c^\dagger(\ddot{\boldsymbol{x}} - \dot{J}_c\dot{\boldsymbol{\theta}}), \tag{2}$$

where $J_c^\dagger$ is the pseudoinverse of J_c. Substituting (2) into (1), we can rewrite the arm dynamics in the task space:

$$\boldsymbol{\tau} = MJ_c^\dagger\ddot{\boldsymbol{x}} + \boldsymbol{N}_c - J_a^\top \boldsymbol{\rho}_a \tag{3}$$

where $\boldsymbol{N}_c = -MJ_c^\dagger\dot{J}_c\dot{\boldsymbol{\theta}} + C\dot{\boldsymbol{\theta}} + N$.

1) Downward Movement: The screwdriver's tip follows a desired trajectory $\boldsymbol{x}_d(t) \in \mathbb{R}^6$ until it establishes contact with the screw's head, while it remains titled during the movement. With the rough estimation of the screw's position, we can set the destination point to be slightly below the plane of the screw's head. Let $\boldsymbol{x}_e = \boldsymbol{x}_d - \boldsymbol{x}$ be the pose error. We employ the following position controller:

$$\boldsymbol{\tau} = MJ_c^\dagger(\ddot{\boldsymbol{x}}_d + k_v\dot{\boldsymbol{x}}_e + k_p\boldsymbol{x}_e + k_i\int \boldsymbol{x}_e dt) + \boldsymbol{N}_c - J_a^\top \boldsymbol{\rho}_a. \tag{4}$$

It is easy to verify that the resulting error dynamics has asymptotic error convergence.

2) Contact Softening: At the moment when the screwdriver's tip contacts the screw's head, the F/T sensor's reading will increase suddenly due to the impact. To soften the impact, we switch from position control in the contact normal direction to impedance control. Let $\{s\}$ be the screw's body frame located at the screw tip's center, such that 1) its z axis coincides with the screw axis and points to the head, and 2) its x axis points to the starting point of the thread. The control objective is to allow the arm's behavior in the z-axis of the screw's frame $\{s\}$ to mimic that of a system with

mass m_o, stiffness k_s, and damping k_d. This target compliant behavior is described as

$$m_o({}^s\ddot{z} - {}^s\ddot{z}_o) + k_d({}^s\dot{z} - {}^s\dot{z}_o) + k_s({}^s z - {}^s z_o) = {}^s f_z \quad (5)$$

where ${}^s z$ and ${}^s f_z$ respectively represent the position and force components in the z-axis of the frame $\{s\}$, and ${}^s z_o$ is the equilibrium position of ${}^s z$ in the absence of ${}^s f_z$.

Under the assumption that the screw is not moving, we have $\ddot{\boldsymbol{x}} = {}^s\boldsymbol{R}^\top {}^s\ddot{\boldsymbol{x}}$, where ${}^s\boldsymbol{R} = \mathrm{diag}({}^sR, {}^sR)$, and ${}^sR$ is the rotation matrix from the world frame to $\{s\}$. Substituting this equation and (2) into (3), we get the arm's dynamics in the screw frame

$$\boldsymbol{\tau} = MJ_c^{\dagger} {}^s\boldsymbol{R}^\top {}^s\ddot{\boldsymbol{x}} + \boldsymbol{N}_c - J_a^\top {}^s\boldsymbol{R}^\top {}^s\boldsymbol{\rho}_a. \quad (6)$$

From (5), we have ${}^s\ddot{z} = {}^s\ddot{z}_o + (k_d {}^s\dot{z}_e + k_s {}^s z_e + {}^s f_z)/m_o$, where ${}^s z_e = {}^s z_o - {}^s z$. We set ${}^s z_o$ to be slightly below the plane of the screw's head so that the contact is maintained throughout the process. For the other five components of ${}^s\ddot{\boldsymbol{x}}$, we apply similar position controls as in (4), except that now all the variables are in the screw frame $\{s\}$. Denote $[\boldsymbol{x}]_i$ as the i-th component of the vector $\boldsymbol{x}$. We obtain the hybrid position-impedance controller for softening the contact by taking the PID servos from (4) into (6), and replacing $[{}^s\ddot{\boldsymbol{x}}]_3$ with $[{}^s\ddot{\boldsymbol{x}}_d]_3 + (k_d[{}^s\dot{\boldsymbol{x}}_e]_3 + k_s[{}^s\boldsymbol{x}_e]_3 + [{}^s\boldsymbol{\rho}_a]_3)/m_o$.

B. Searching for the Screw Drive

In a most likely scenario, the screwdriver's tip does not go inside the screw's drive directly when it lands on the screw head. Our next step is to search for the drive by sliding the tip on the surface of the screw's head. Here we describe a search strategy[1] that uses two orthogonal straight sliding paths l_1 and l_2 as shown in Fig. 2(a).

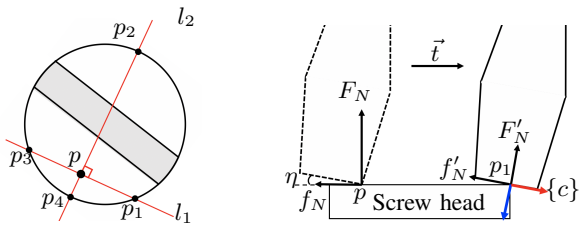

(a) (b)

Fig. 2: Search for the drive: (a) two orthogonal sliding paths l_1 and l_2 for the screwdriver's tip; (b) tip sliding on the head along $\overrightarrow{pp_1}$ to reach an edge. $\vec{t}$ denotes the moving direction, which aligns the tip tilting direction.

1) Drive Search: Let p be the initial contact point of the tip and the screw's head and l_1 be the line that is parallel to the projection of the screwdriver's tip edge (x-axial direction in the screwdriver's body frame) onto the plane of the screw head. The tip first slides along l_1 in the direction that it tilts to (say $\overrightarrow{pp_1}$ in Fig. 2(a)) until it encounters the drive or reaches the head's boundary. If no drive is discovered, the tip reverses its sliding direction along l_1 and moves back to p. At p, the tip rotates counterclockwise for 90 degrees to align the tilting direction with l_2, and then moves along $\overrightarrow{pp_2}$. In the worst case, the drive search is done in four directions with the order of $\overrightarrow{pp_1}$, $\overrightarrow{pp_2}$, $\overrightarrow{pp_3}$, and $\overrightarrow{pp_4}$ specifically.

The control objective is to make the tip track l_1 and l_2 while maintaining a stable contact force at the same time. A sudden change in the contact force will indicate contact with either an edge of the drive or the head's boundary. Sliding is carried out under hybrid position/force control in the screw's body frame as described in equation (4) by setting $[{}^s\ddot{\boldsymbol{x}}]_3 = 0$, which is ensured by the fact that the tip is moving on the surface of the screw's head. We apply force control in the body fame's z-direction by replacing $[{}^s\boldsymbol{\rho}_a]_3$ in (6) with a servo $f_d + k_p f_e + k_i \int f_e dt$, where $f_e = f_d - [{}^s\boldsymbol{\rho}_a]_3$.

2) Prevention of Sliding off the Screw Head: Sliding of the tip ends in one of two situations: 1) it reaches one of the drive's straight edges; and 2) it reaches the circular boundary of the screw head (see Fig. 2(b)). In both situations the contact will experience a sudden change that will be captured by the F/T sensor located at the end-effector.

When an edge e is encountered, it is important to stabilize the tip (and the screwdriver) instantly. At the instant, the point-surface contact between the tip point and the head immediately switches to one between the edge e and the screwdriver's tip edge. This allows time to stop the tip's movement and prevent it from sliding off the edge.

Control is done in a frame $\{c\}$ attached to the screw as shown in Fig. 2(b), such that its x and z axes align with the bottom tip edge and screwdriver axis respectively. We use impedance control with the same target compliant behavior as (5) by replacing $[{}^c\ddot{\boldsymbol{x}}]$, for $1 \le i \le 3$, with the servo $[{}^c\ddot{\boldsymbol{x}}_d]_i + (k_d[{}^c\dot{\boldsymbol{x}}_e]_i + k_s[{}^c\boldsymbol{x}_e]_i + [{}^c\boldsymbol{\rho}_a]_i)/m_o$. The screwdriver's orientation, represented by the Euler angles, is placed under position control. The arm dynamics in the frame $\{c\}$ is similar to (6) with the replacement of ${}^sR$ by ${}^cR$.

3) Edge Discrimination: We cannot distinguish a drive edge from the head boundary by the change in force direction alone because the relative orientation of the screwdriver's tip and the screw is unknown. Let the screwdriver continue the movement in its current direction. If it has encountered a drive edge, there will be a second change in the force direction when the tip contacts the opposite edge of the drive. On the other hand, if there is no such change within a short distance, say δ, of movement, the tip has reached the circular boundary of the screw head.

To realize the above movement, we can switch to position control in the x-direction of the frame $\{c\}$ with a desired constant velocity to move the distance of δ. The remaining five directions are placed under the same control applied to stabilize the tip at the boundary when searching for the drive earlier.

C. Tip Insertion

Once the tip is inside the drive and makes contact with its two edges, it needs to be fully inserted to be ready for fastening. Denote by $\{c'\}$ the instantaneous frame located at the tip contact in the same orientation as the screwdriver. It

[1]The initial idea was conceived by Shengwen Xie.

is located at the current tip position. Both the orientation and location can be calculated from the joint angles via forward kinematics. This insertion is carried out in a sequence of three rotations to be described below.

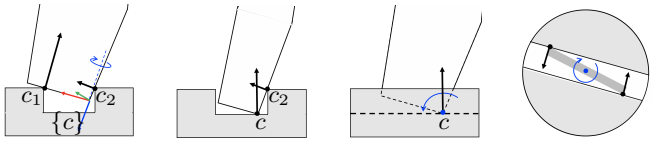

(a) (b) (c) (d)

Fig. 3: Tip insertion: (a) rotate about the z-axis of the frame $\{c\}$ while maintaining the two contact points c_1 and c_2; (b) the contact at c_1 disappears and the tip falls inside the drive; (c) rotate to align the axis of the screwdriver with that of the screw; (d) rotate about the screwdriver's axis and get to the final configuration.

First, the screwdriver rotates about its axial direction while maintaining the two contact points, under control in its body frame. We use a simple position controller for this rotation. In the translational x and y directions, we still employ impedance control, except that now the equilibrium point is set on the x-axis slightly into the drive edge in order to maintain the contact at c_2. In the z-direction, a constant force F_1 is maintained at c_1. When the contact at c_1 disappears during the rotation, a change of force can be detected by the sensor, indicating that the entire tip is inside the drive. At this moment, the frictional force at c_2 will be unable to counter the force that the robot applies in the z direction. Therefore, the tip will drop into the drive, generating an impact that can be softened via impedance control in the downward direction.

Next, the screwdriver is rotated until its axis becomes parallel to the screw's axis, along which the contact force is maintained. Then, the screwdriver is centered in the drive based on the position of the screw.

Finally, an axial rotation of the screwdriver is carried out until a torque is sensed in the axial direction. At this moment, the screwdriver is well-positioned and ready to start driving the screw.

D. Null Space Control

Rotations to carry out tip insertion and screw driving can go out of the joint limits of the robotic arm. If the arm has extra degrees of freedom, null space control can be applied to reduce the chance of a joint limit being exceeded.

The null space of the Jacobian J_c at the tip-drive contact point c characterizes all the joint motions that have no effect on the screw driving task. We can construct an artificial potential field function [34] $V(\boldsymbol{\theta}) = k\sum_{i=1}^{n}\left(\theta_i - \frac{\theta_{i_{\min}}+\theta_{i_{\max}}}{2}\right)^2$, where θ_i is the i-th joint angle, $\theta_{i_{\min}}$ and $\theta_{i_{\max}}$ represent the lower and upper limits of the i-th joint respectively. We can add an extra term $\tau_{\text{null}} = (I_n - J_c^{\dagger}J_c)\tau_0$ to our controller, where $\tau_0 = -\nabla V(\boldsymbol{\theta})$. This will guide the joint movement in the null space of J_c with the tendency to minimize $V(\boldsymbol{\theta})$. This helps to keep each every joint angle θ_i in the middle of its range.

III. SCREW DRIVING

The next step is to control the mounted screwdriver to drive the screw. We assume that the screwdriver's tip does not slide inside the drive due to enough contact friction. This assumption can be achieved by maintaining a force on the screw head by the screwdriver in the z-direction of the contact frame.

A. Force/Torque Modeling

To control the arm (and the attached screwdriver), the interaction between the screw and the threaded hole needs to be modeled. This comes down to computation of the force and torque received by the screw due to its penetration into the hole.

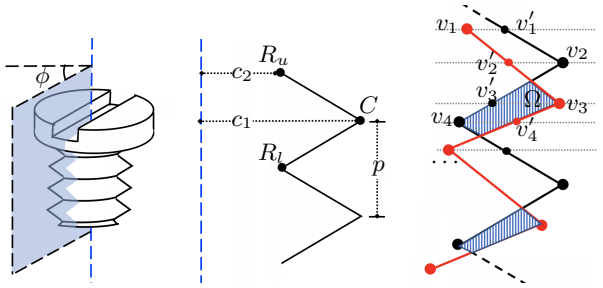

(a) (b) (c)

Fig. 4: Modeling the screw-hole interaction: (a) cross section within a plane through the screw axis; (b) triangular element $\triangle R_u C R_l$ in the cross section; and (c) its penetration into the walls of the hole. The red and black lines represent the cross sections of the screw and the hole respectively.

Consider the thread of the screw as the trajectory of a triangular element (see Fig. 4(b)). The three vertices of this triangle move along separate helix curves: the crest curve $\boldsymbol{c}(\phi) = \left(c_1\cos\phi, -c_1\sin\phi, \frac{\phi}{2\pi}p\right)^{\top}$, and the upper/lower root curve $\boldsymbol{r}_{u/l}(\phi) = \left(c_2\cos\phi, -c_2\sin\phi, \frac{\phi}{2\pi}p \pm \frac{p}{2}\right)^{\top}$, where ϕ is the amount of the rotation along the helix curve, c_1 is the major radius (distance from the crest to the screw/hole axis), c_2 is the minor radius (distance from the root), and p denotes the pitch.

Let $\{s\}$ be the screw's body frame as described in II-A.2. The hole's frame $\{h\}$ locates at the center of the hole's plane, with z axis pointing into the hole, and x axis similarly defined as $\{s\}$. The coordinates of the three points in each thread element in the frame $\{s\}$ or $\{h\}$ can be easily calculated from $\boldsymbol{c}(\phi)$ and $\boldsymbol{r}_{u/l}(\phi)$.

Figure 4(c) illustrates the thread engagement between the screw and the hole in the plane through the screw axis as determined by the angle ϕ. We can calculate all the vertices on the hole's thread within the cross section by taking $\phi+2i\pi$ into the functions of $\boldsymbol{c}(\phi)$ and $\boldsymbol{r}_{u/l}(\phi)$. Due to the slight tilting of the screw, the plane containing the axial cross section at ϕ of the screw may not coincide with the hole's plane at ϕ. However, this error is small enough to be ignored. So, we use the same functions to get the vertices on the screw

threads, and transform the coordinates in $\{s\}$ into $\{h\}$ by their relative pose.

As shown in Fig. 4(c), the intersections of the screw thread and the hole thread in the same plane appear at most once between the vertices. Therefore, with all the vertices known, we can do a plane sweep to calculate the penetration area efficiently. As we walk along the vertices on both threads from top to bottom, it is easy to check if the screw penetrates into the wall or not at each vertex v_i by comparing with the point on the other thread at the same height (see Fig. 4(c)). This check is discussed with details in [35]. Three cases may arise: 1) the screw penetrates into the wall at v_i but not at v_{i+1}, which means that an intersection happens; 2) the screw penetrates at v_i but not at v_{i+1}, which suggests the end of an intersection; 3) both v_i and v_{i+1} have the same condition, which implies that there is no change of intersection. We can calculate the area A of the penetration region Ω. This allows us to estimate the force based on the area using a simple spring model $F = kA$, where k is a stiffness constant, and apply the force at the center of Ω in a direction normal to its upper or bottom edge (depending on the center of Ω). With all the normal forces determined along the threads, the frictional forces and the torques can be determined. Finally, we integrate all the forces and torques for all cross sections over $\phi = [0, 2\pi)$ to obtain the force and torque exerted on the screw from the hole.

B. Hybrid Control for Torquing

The screw moves a distance of $\Delta d = (p \times \Delta\theta)/2\pi$ along the hole's axis, where p is the pitch of the threads, and $\Delta\theta$ is the amount of the screw's rotation about the hole's axis. Differentiating this equation and representing it in terms of the state variable $\boldsymbol{x}$, we get $[{}^h\dot{\boldsymbol{x}}]_z = \frac{p}{2\pi}[{}^h\boldsymbol{\omega}]_z$ where ${}^h\boldsymbol{\omega} \in \mathbb{R}^3$ is the angular velocity of the screw in the hole frame $\{h\}$ as defined earlier. The state variable is $\boldsymbol{h} = [{}^hx, {}^hy, {}^h\alpha, {}^h\beta, {}^h\gamma]^\top$. Here, ${}^hx$ and ${}^hy$ give the tangential displacements between the centers of the screw's head and the hole in the frame $\{h\}$, and $({}^h\alpha, {}^h\beta, {}^h\gamma)$ are the z-y-x Euler angles of the screw frame $\{s\}$ relative to the hole frame $\{h\}$. From the relationship between $[{}^h\dot{\boldsymbol{x}}]_z$ and $[{}^h\boldsymbol{\omega}]_z$, we get the screw's velocity as

$$ {}^h\boldsymbol{v} = \begin{bmatrix} 1 & 0 & 0 & 0 & 0 \\ 0 & 1 & 0 & 0 & 0 \\ 0 & 0 & 0 & 0 & p/2\pi \\ 0 & 0 & 1 & 0 & 0 \\ 0 & 0 & 0 & 1 & 0 \\ 0 & 0 & 0 & 0 & 1 \end{bmatrix} \begin{bmatrix} I_2 & \mathbf{0} \\ \mathbf{0} & S \end{bmatrix} \dot{\boldsymbol{h}} \tag{7} $$

where S is a matrix that transforms Euler angle rates to the angular velocity. We let Σ and T denote the first two matrices on the right hand side of the above equation. It follows from the arm kinematics that ${}^h\boldsymbol{v} = J_h\dot{\boldsymbol{\theta}}$, where ${}^h\boldsymbol{v} = [{}^hv_p, {}^hv_r]^\top$ gives the translational and angular velocities in the frame $\{h\}$, and J_h is the Jacobian matrix that transfers joint angle rates to ${}^h\boldsymbol{v}$. From (7), we obtain $\dot{\boldsymbol{h}} = T^{-1}\Sigma^\dagger J_h\dot{\boldsymbol{\theta}}$. Differentiating this equation, and substituting the result into the arm dynamics in the frame $\{h\}$, we get the dynamics expressed in the task coordinates $\boldsymbol{h}$.

For rotation about the hole's axis, we simply use a PID position control to track a desired trajectory specified by the rotation angle as a function of time, say $\theta(t) = [\boldsymbol{\omega}_d]_z t$, where $\boldsymbol{\omega}_d = [0, 0, \dot{\theta}]^\top$ is the desired angular velocity. For translational and rotational movements in the tangential directions (i.e., four directions represented by ${}^h\boldsymbol{p} = [{}^hx, {}^hy, {}^h\alpha, {}^h\beta]^\top$), we use the modeled force/torque components in those directions to keep the screw's axis from any sizable deviation from the hole's. This is realized via admittance control to make the robot yield to the force/torque with a movement in each corresponding direction. The target compliant behavior is

$$ \boldsymbol{M}_o({}^h\ddot{\boldsymbol{p}}_d - {}^h\ddot{\boldsymbol{p}}) + \boldsymbol{K}_d({}^h\dot{\boldsymbol{p}}_d - {}^h\dot{\boldsymbol{p}}) + \boldsymbol{K}_s({}^h\boldsymbol{p}_d - {}^h\boldsymbol{p}) = -{}^h\boldsymbol{f} $$

where ${}^h\boldsymbol{f}$ is the combined force and torque in the tangential directions of $\boldsymbol{\rho}_a$. From the equation above, we solve for ${}^h\ddot{\boldsymbol{p}}_d$. The desired trajectories ${}^h\dot{\boldsymbol{p}}_d$ and ${}^h\boldsymbol{p}_d$, obtained through integration of ${}^h\ddot{\boldsymbol{p}}_d$, are then used for position control in the task space within the frame $\{h\}$.

In addition to controlling the state variable f$\boldsymbol{h}$, we also need to maintain a force in in the z-direction of the frame $\{h\}$ to prevent the screwdriver's tip from slipping out of the drive or the screw's threads from being damaged.

IV. SIMULATION

Simulation is conducted on the platform MuJoCo with a 7-DOF KUKA LBR iiwa robot[2]. The setup is shown in Fig. 5(a). This section presents a successful execution of screwdriver mounting and screw driving (with accompanying video as a supplement).

A. A Full Execution of Mounting and Torquing

Mounting starts with the screwdriver moving down to establish a point-surface contact with the head (Fig. 5(b)), and the tilting angle of the tip is $\pi/10$.

Then it does a drive search as described in II-B.1. When the sensor detects a change of force direction (0.2115 rad in Fig. 5(c)), impedance control is activated to prevent it from sliding off the edge. In Fig. 5(d), the tip slides along the edge, classifying it as a head boundary. The search direction then changes as described in II-B.1. The next search follows l_2 to discover the drive in Fig. 5(g). Throughout the drive search, the force in the normal direction of the contact frame is maintained in the range 1 ± 0.03 N.

Fig. 6 shows the insertion of the tip. During the first rotation in (a)–(b) , the employed hybrid controller maintains a contact force (2 ± 0.05 N) at c_1 in the negative z-direction, and a contact force (0.5 ± 0.1 N) at c_2 in positive x-direction (cf. Fig. 3). A torque of 0.01 Nm in the screwdriver axial

[2]The screw parameters include: 1) pitch $p = 1.30$ mm; 2) drive width $w = 2.00$ mm; 3) major radius $c_1 = 0.50$ mm; and 4) minor radius $c_2 = 0.38$ mm. The parameter for the hole is scaled according to the screw with 1.07. The control parameters include: 1) $K_p = 400$, $K_v = 35$, $K_i = 500$ (position control); 2)$k_p = 20$, $k_i = 250$ (force control); 3) $m_o = 10$, $k_d = 200$, $k_s = 50$ (impedance control); and 4) $M_o = 10$, $K_d = 4000$, $K_s = 100$ (admittance control).

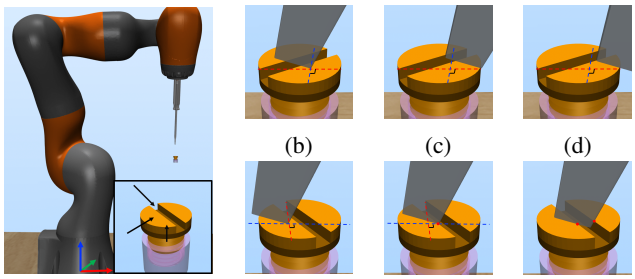

Fig. 5: Search for the screw drive: (a) simulation setup; (b)–(d) the search along the line l_1 (red) reaches the boundary of the screw head; (e)–(g) the next search along along the orthogonal line l_2 (blue) finds the drive.

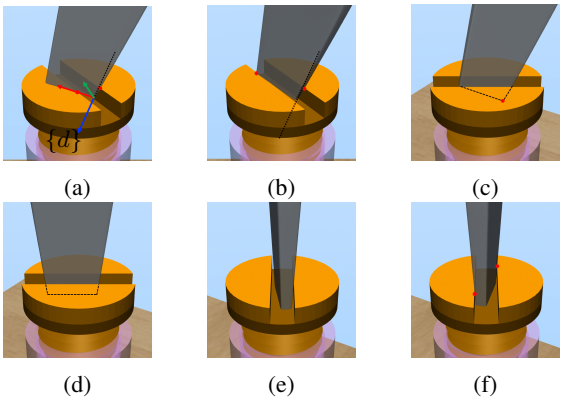

Fig. 6: Three rotations to insert the tip: (a)–(b) about the z-axis of the frame $\{d\}$, whose z and x axes are parallel to the screwdriver's axis and shaft edge respectively; (c)–(d) about the direction perpendicular to the shaft; and (e)–(f) about the screwdriver's axis.

direction is sensed when the configuration shown in (f) is reached. During the last two rotations, a force in the range 1 ± 0.03 N along the normal direction of the contact frame is maintained to prevent contact loss.

The initial configuration in Fig. 7(a) is the same as that in Fig. 6(f). The robot configuration is reset in (c) by rotating the screwdriver counterclockwise through π. With drive's orientation known before the disengagement, the tip is easily inserted back to start torquing in the next round. The force in the screwdriver's axial direction is maintained within 5 ± 0.02 N, and the torque increases from 0.0107 Nm in (a) to 0.0145 Nm in (d). Meanwhile, impedance control applied in the orthogonal directions will keep the force in range ± 0.03 N.

B. Results

For further testing, we have conducted twenty simulation trials for each of screwdriver mounting and screw driving operations. Each trial randomly selects the position of the screw in a 0.05 m box centered at $(0.3, 0.0, 0.4)$ m, and the direction of the drive from $[0, 2\pi)$.

All the twenty trials on mounting can identify the drive, but only fifteen of them end up with successful tip insertions.

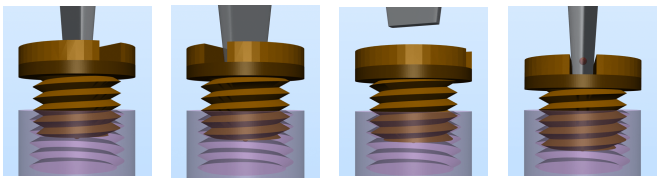

Fig. 7: Screw driving: (a) initial configuration; (b) clockwise rotation through $\pi/3$; (c) disengagement of the screwdriver when reaches the joint limits after a torquing through $4\pi/5$. through $12\pi/15$. ; and (d) configuration after two iterations.

Five trials fail because a joint of the arm has reached its limit to prevent the robot from completing a specific rotation for tip insertion. It is possible to avoid this type of failure by using a different initial configuration and planning a better rotation trajectory. Among the successful trials, the time for mounting task varies from 50 to 110 seconds, as affected by the drive search.

All the twenty trials on screw driving have seen the completion of three iterations of the following steps: torquing, disengagement, joint reset, and insertion again. The average time for a complete iteration is 15 seconds.

It is worth mentioning that when null space control is not activated, most of the trials would fail easily on a rotation (during either tip insertion or screw driving). For example, when the robot tries to rotate the screwdriver about its axis, there is a tendency of using only the first six joints of a 7-DOF KUKA instead of the last joint whose axis coincides with the screwdriver.

V. DISCUSSION AND FUTURE WORK

This paper presents control policies for mounting a screwdriver and using it to tighten a screw. The mounting strategy solves a generalized peg-in-hole problem by combining a sliding-based search for the screw drive with controlled rotations that utilize compliance for tool tip alignment and insertion. Installation of the virtual fence around the screw's head carries a good promise for mating of small parts. The tightening strategy maintains the axial alignment of the screw and the threaded hole based on modeling and regulating their interactions. Various control policies, over position, impedance, and admittance, are integrated smoothly to execute this fine manipulation task.

The work needs to be extended in several directions to approach the skill level of screw driving by the human hand. Clearly, the screwdriver should be held and maneuvered by a robotic hand (mounted on a robotic arm). This leads to issues of tool pickup, maneuver, and exchange, all of which rely on execution of finger gaits involving contact establishment, maintenance, and disengagement. Impedances between the fingertips and the screwdriver and between the screwdriver and the screw need will serve an important role during the fastening action. Effective finger and screwdriver control policies will require more accurate modeling of the screw-substrate contact force, which cannot be sensed directly.

REFERENCES

[1] Antonio Bicchi and Vijay Kumar. Robotic grasping and contact: A review. In *Proc. IEEE Int. Conf. Robot. Autom.*, 2000, pp. 348–353.

[2] Antonio Bicchi. Hands for dexterous manipulation and robust grasping: a difficult road toward simplicity. *IEEE Trans. Robot. Autom.*, vol. 16, no. 6, pp. 652–662, 2000.

[3] A. M. Okamura, N. Smaby, and M. R. Cutkosky. An overview of dexterous manipulation. In *Proc. IEEE Int. Conf. Robot. Autom.*, 2000, pp. 255–262.

[4] Ingo Kresse, Ulrich Klank, and Michael Beetz. Multimodal autonomous tool analyses and appropriate application. In *IEEE-RAS Int. Conf. Humanoid Robots*, 2011, pp. 698–613.

[5] V. Tikhanoff, U. Pattacini, L. Natale, and G. Metta. Exploring affordances and tool use on the iCub. In *IEEE-RAS Int. Conf. Humanoid Robots*, 2013, pp. 130–137.

[6] S. Gupta, C. J. Paredis, and P. Brown. Micro planning for mechanical assembly operations. In *Proc. IEEE Int. Conf. Robot. Autom.*, 1998, pp. 239–246.

[7] M. Toussaint, K. Allen, K. A. Smith, and J. B. Tenenbaum. Differentiable physics and stable modes for tool-use and manipulation planning. In *Robot. Sci. Syst.*, 2018.

[8] Wenbin Li and Mario Fritz. Teaching robots the use of human tools from demonstration with non-dexterous end-effectors. In *IEEE-RAS Int. Conf. Humanoid Robots*, 2015, pp. 547–553, .

[9] N. Saito, K. Kim, S. Murata, T. Ogata, and S. Sugano. Tool-use model considering tool selection by a robot using deep learning. In *IEEE-RAS Int. Conf. Humanoid Robots*, 2018, pp. 270–276.

[10] K. Fang, Y. Zhu, A. Garg, A. Kurenkov, V. Mehta, Li Fei-Fei, and S. Savarese. Learning task-oriented grasping for tool manipulation from simulated self-supervision. *Int. J. Robot. Res.*, vol. 39, no. 2–3, pp. 202–216, 2020.

[11] Tsutomu Hasegawa, Takashi Suehiro, and Kunikatsu Takase. A model-based manipulation system with skill-based execution. *IEEE Trans. Robot. Autom.*, vol. 8, no. 5, pp. 535–544, 1992.

[12] Heiko Hoffmann, Zhichao Chen, Darren Earl, Derek Mitchell, Behnam Salemi, and Jivko Sinaopv. Adaptive robotic tool use under variable grasps. *Robot. Autom. Syst.*, vol. 62, pp. 833–846, 2014.

[13] Jörg Stückler and Sven Behnke. Adaptive tool-use strategies for anthropomorphic service robots. In *IEEE-RAS Int. Conf. Humanoid Robots*, 2014, pp. 755–760.

[14] Zhenzhong Jia, Ankit Bhatia, Reuben M. Aronson, David Bourne, and Matthew T. Mason. A survey of automated threaded fastening. *Trans. Autom. Sci. Eng.*, vol. 16, no. 1, pp. 298–310, 2019.

[15] Bruno Lara, Kaspar Althoefer, and Lakmal D. Seneviratne. Automated robot-based screw insertion system. In *Proc. 24th Annu. Conf. IEEE Ind. Electron. Soc.*, 1998, pp. 2440–2445.

[16] S. Pitipong, P. Pornjit, and P. Watcharin. An automated four-DOF robot screw fastening using visual servo. In *Proc. IEEE/SICE Int. Symp. Syst. Integr.*, pp. 379–383, 2010.

[17] M. A. Diftler and Ian D. Walker. Experiments in aligning threaded parts using a robot hand. *IEEE Trans. Robot. Autom.*, vol. 15, no. 5, pp. 858–868, 1999.

[18] D. E. Whitney. Quasi-static assembly of compliantly supported rigid parts. *ASME J. Dynam. Syst. Meas. Control*, vol. 104, pp. 65–76, 1982.

[19] H. Bruyninckx, S. Dutre, and J. De Schutter. Peg-on-hole: a model based solution to peg and hole alignment. In *Proc. IEEE Int. Conf. Robot. Autom.*, 1995, pp. 1919–1924.

[20] J. F. Broenink and M. L. Tiernego. Peg-in-hole assembly using impedance control with a 6-DOF robot. In *Proc. 8th Eur. Simul. Symp.*, 1996, pp. 504–508.

[21] Te Tang, Hsien-Chung Lin, Yu Zhao, Wenjie Chen, and Masayoshi Tomizuka. Autonomous alignment of peg and hole by force/torque measurement for robotic assembly. In *Proc. IEEE Int. Conf. Autom. Sci. Eng.*, 2016, pp. 162–167.

[22] H. Park, J. Park, D.-H. Lee, J.-H. Park, M.-H. Baeg, and J.-H. Bae. Compliance-based robotic peg-in-hole assembly strategy without force feedback. *IEEE Trans. Ind. Electron.*, vol. 64, no. 8, pp. 6299–6309, 2017.

[23] M. Raibert and J. Craig. Hybrid position/force control of manipulators. *ASME J. Dynam. Syst. Meas. Control*, vol. 103, no. 2, pp. 126–133, 1981.

[24] Neville Hogan. Impedance control: An approach to manipulation: Parts I — III. *ASME J. Dynam. Syst. Meas. Control*, vol. 107, pp. 1–24, 1985.

[25] Edward J. Nicolson and Ronald S. Fearing. Dynamic modeling of a part mating problem: Thtreaded fasterner insertion. In *Proc. IEEE/RSJ Int. Conf. Intell. Robots Syst.*, 1991, pp. 30–37.

[26] L. Seneviratne, F. Ngemoh, and S. Earles. Theoretical modeling of screw tightening operations. In *Proc. ASME Eur. Joint Conf. Syst. Des. Anal.*, 1992, pp. 189–192.

[27] L. Seneviratne, F. Ngemoh, S. Earles, and K. A. Althoefer. Theoretical modeling of the self-tapping screw fastening process. *J. Mech. Eng. Sci.*, vol. 215, no. 2, pp. 135–154, 2001.

[28] Stephen Wiedmann and Bob Sturges. Spatial kinematic analysis of threaded fastener assembly. *ASME J. Mech. Des.*, vol. 128, pp. 116-127, 2006.

[29] Stephen Wiedmann and Bob Sturges. A full kinematic model of thread-starting for assembly authomation analysis. *ASME J. Mech. Des.*, vol. 128, no. 128–136, 2006.

[30] Takeshi Tsujimura and Tetsuro Yabuta. Adaptive force control of screwdriving with a positioning-controlled manipulator. *Robot. Autom. Syst.*, vol. 7, pp. 57–65, 1991.

[31] Edward J. Nicolson and Ronald S. Fearing. Compliant control of threaded fastener insertion. In *Proc. IEEE Int. Conf. Robot. Autom.*, 1993, pp. 484–490.

[32] N. Dhayagude, Z. Gao, and F. Mrad. Fuzzy logic control of automated screw fastening. *Robot. Comput.-Integr. Manuf.*, vol. 12, no. 3, pp. 235–242, 1996.

[33] Kai Pfeiffer, Adrien Escande, and Abderrahmane Kheddar. Nut fastening with a humanoid robot. In *Proc. IEEE/RSJ Int. Conf. Intell. Robots Syst.*, 2017, pp. 6141–6148.

[34] Oussama Khatib. Inertial properties in robotic manipulation: An object-level framework. *Int. J. Robot. Res.*, vol. 14, no. 4, pp. 19-36, 1995.

[35] E. J. Nicolson and R. S. Fearing, Dynamic modeling of a part mating problem: threaded fastener insertion. *Int. Conf. Intell. Robots Syst.*, 1991, pp. 30–37.